# Energetics of the exchangeable quinone, Q B , in Photosystem II

Sven de Causmaecker, Jeffrey Douglass, Andrea Fantuzzi, Wolfgang Nitschke, A. William Rutherford

# Energetics of the exchangeable quinone, $Q_B$, in Photosystem II

De Causmaecker, S.[1], Douglass J.[1], Fantuzzi A.[1], Nitschke W.[2] and Rutherford A.W.[1]

1) Department of Life Sciences, Imperial College London, SW7 2AZ London, UK.
2) Aix Marseille Univ, CNRS, BIP/UMR7281, Marseille, France.

## Abstract

Photosystem II (PSII), the light-driven water/plastoquinone photo-oxidoreductase, is of central importance in the planetary energy cycle. The product of the reaction, plastohydroquinone ($PQH_2$), is released into the membrane from the $Q_B$-site, where it is formed. A plastoquinone (PQ) from the membrane pool then binds into the $Q_B$-site. The thermodynamic properties of the PQ in the $Q_B$-site, $Q_B$, in its different redox forms have received relatively little attention despite their functional importance. Here we report the midpoint potentials ($E_m$) of $Q_B$ in PSII from *Thermosynechococcus elongatus* using EPR spectroscopy: $E_m(Q_B/Q_B^{\bullet-}) \approx 90$ mV and $E_m(Q_B^{\bullet-}/Q_BH_2) \approx 40$ mV. These data allow the following conclusions: 1) the semiquinone, $Q_B^{\bullet-}$, is thermodynamically stable under physiological conditions; 2) release of $Q_BH_2$ ($PQH_2$) into the pool has a driving force of ~50 meV; 3) PQ is more tighly bound than $PQH_2$; 4) the difference between the $E_m$ values for $Q_B/Q_B^{\bullet-}$ and $Q_A/Q_A^{\bullet-}$ is ~234 meV and represents the driving force for electron transfer from $Q_A^{\bullet-}$ to $Q_B$. We also used the pH-dependence of the thermoluminescence associated with $Q_B^{\bullet-}$ to provide a functional estimate for this energy gap and obtained a similar value (~230 meV). This estimate is larger than the generally accepted value (~80 meV). The energetics of $Q_B$ are compared to those in homologous purple bacterial reaction centers. A recent contradictory report on the redox properties of $Q_B$ (Kato Y, Nagao R, Noguchi T 2016 *Proc Natl Acad Sci* 113(3):620–625) is rationalised in terms of specific technical difficulties associated with titrating an exchangeable cofactor.

## Introduction

In photosynthesis sunlight is absorbed by chlorophyll molecules resulting in charge separation within a photosynthetic reaction center. In Photosystem II (PSII), the water/plastoquinone photo-oxidoreductase, the electron hole is transferred from the chlorophyll cation radical, $P_{D1}^{\bullet+}$, via a redox active tyrosine ($Tyr_Z$) to the $Mn_4O_5Ca$ cluster. After four sequential photochemical turnovers and the resulting oxidations of the $Mn_4O_5Ca$ cluster ($S_{0-4}$), two water molecules are oxidized (1). On the electron-acceptor side, the electron is transferred from the pheophytin anion ($Pheo_{D1}^{\bullet-}$) via a

non-exchangeable plastoquinone ($Q_A$), which acts as a 1-electron relay, to an exchangeable plastoquinone ($Q_B$), the terminal electron acceptor (2).

The formation of $Q_B^{\bullet-}$ is stabilized by the protonation of a near-by amino acid. $Q_B^{\bullet-}$ decays in the tens of seconds timescale by charge recombination with $S_2$ or $S_3$ when present, but is stable for several hours if $S_0$ or $S_1$ are present (3). During the subsequent photochemical turnover, $Q_B^{\bullet-}$ accepts a second electron from the newly-formed $Q_A^{\bullet-}$. This is accompanied by the two protonation steps, thought to occur sequentially, one before and one after the arrival of the second electron (4), as occurs in the homologous site in purple bacteria (5). The $Q_BH_2$ formed is released from the site and enters the $PQ/PQH_2$ pool, from where it can deliver electrons to the cytochrome *$b_6f$* complex (6–8).

Due to the two-electron chemistry of $Q_B$, the $Q_B^{\bullet-}$ state is the only state on the electron acceptor side that cannot be stabilized by forward electron transfer, there is no "kinetic control" on this step (9). It is therefore available to back-react via $Q_A^{\bullet-}$ with the $S_2$ and $S_3$ states on the donor side (3). Two main competing back-reaction pathways occur within PSII: 1) the direct route via electron tunnelling from $Q_A^{\bullet-}$ to $P^{\bullet+}$; and 2) the indirect route via thermal repopulation of the $P^{\bullet+}Pheo_{D1}^{\bullet-}$ state (10). Recombination from the $P^{\bullet+}Pheo_{D1}^{\bullet-}$ state mainly forms the triplet chlorophyll state $^3P_{680}$ (11), which reacts with oxygen to form highly reactive and damaging singlet oxygen $^1O_2$ (12).

The driving force ($\Delta G$) for electron transfer between $Q_A$ and $Q_B$ determines the $Q_A^{\bullet-}Q_B \leftrightarrow Q_AQ_B^{\bullet-}$ equilibrium and therefore the extent to which back-reactions from $Q_B^{\bullet-}$ (or $Q_BH_2$) to $Q_A$ can occur. This equilibrium is determined by the difference between $E_m(Q_A/Q_A^{\bullet-})$ and $E_m(Q_B/Q_B^{\bullet-})$ or $E_m(Q_B^{\bullet-}/Q_BH_2)$ according to the following equation:

$$\Delta G = -nF(\Delta E) \qquad \text{(Eq. 1)}$$

The redox state of $Q_A$ can be monitored relatively easily using fluorescence measurements and a wide range of different values have been reported (13). This scatter of reported values is at least in part due to the potential being modulated to regulate forward and particularly back electron transfer reactions (9). The $Q_A$ redox potential is affected by the binding of the $Mn_4O_5Ca$ cluster to its site (10, 13–15) and by the bicarbonate binding to the non-heme iron (16) (see Figure 1). The redox potential of the $Q_A/Q_A^{\bullet-}$ couple in the fully functional, bicarbonate-bound system is −144 mV (15, 16).

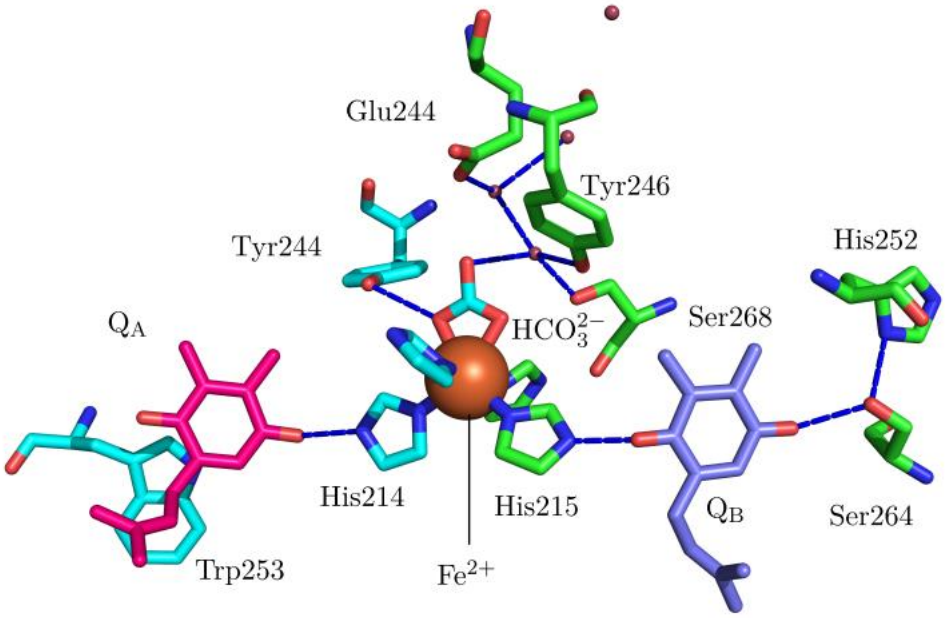


Figure 1: PSII acceptor side. Data from the 1.9 Å crystal structure (PDB id: 3WU2)(17)

The measurement of the redox state of $Q_B$ is more complicated than that of $Q_A$. Firstly, there is no easy experimental probe for the redox state of $Q_B$. Secondly, in contrast to $Q_A$, which undergoes a one-electron redox reaction forming $Q_A^{\bullet-}$ without the involvement of protons, the $Q_B$ reduction involves two electrons and two protons (see Eq. 2).

$$Q_B + e^- + H^+ \leftrightarrow Q_B^{\cdot-}(H^+) + e^- + H^+ \leftrightarrow Q_B H_2 \qquad \text{(Eq. 2)}$$

Thirdly, $Q_A$ is a tightly bound cofactor in both of its redox states, while $Q_B$ has two of the three relevant redox states, $Q_B$ and $Q_BH_2$, that are relatively weakly bound and exchangeable with PQ or $PQH_2$. As a consequence, for decades kinetic data were used to estimate the redox potential of $Q_B$ by deriving the equilibrium constants for the electron transfer from $Q_A^{\bullet-}$ to $Q_B$ and $Q_B^{\bullet-}$ (18–20). Due to the complex nature of the experiments from which those kinetic parameters were extracted, uncertainties remain within the literature (18–21). Estimates from a theoretical model based on thermoluminescence data were used to obtain the difference in energy between the $Q_A/Q_A^{\bullet-}$ and $Q_B/Q_B^{\bullet-}$ couples. While this model has proven insightful when used in a qualitative or comparative way, the relationship between experimental observables and thermodynamic parameters derived from this model have not been firmly established (22–24).

An experimental estimate of the two couples based on equilibrium redox titrations was published recently (25). FT/IR was used to monitor $Q_B^{\bullet-}$ formation upon illumination by a single flash as a function of the applied potential. The data showed that $Q_B^{\bullet-}$ was not thermodynamically stable, a surprising result, in light of the better-known homologous purple bacterial reaction centers (21, 26–28).

In summary, the mechanism and energetics of the PSII acceptor side and especially $Q_B$ are still relatively poorly understood. Specifically, the redox potentials for the two couples, $E_m(Q_B/Q_B^{\bullet-})$ and $E_m(Q_B^{\bullet-}/Q_BH_2)$, which are central to understanding charge stabilisation and recombination, have received relatively little attention.

Here we have used EPR spectroscopy to determine the redox potential of the two couples $Q_B/Q_B^{\bullet-}$ and $Q_B^{\bullet-}/Q_BH_2$. Two different EPR signals were measured: a $Q_B^{\bullet-}Fe^{2+}$ semiquinone signal (29) and a $Q_A^{\bullet-}Fe^{2+}Q_B^{\bullet-}$ biradical signal (30, 31). We also used thermoluminescence to determine empirically the energy gap between the $Q_A/Q_A^{\bullet-}$ and $Q_B/Q_B^{\bullet-}$ couples, without relying on the theoretical model previously employed. Our results differ from previous measurements and estimates and show that the semiquinone $Q_B^{\bullet-}$ is highly stabilized thermodynamically and that the plastoquinone is preferentially bound compared to the plastoquinol.

## Results

EPR spectra of PSII were measured at a series of electrode potentials. The D2-Y160F mutant lacking tyrosine D ($Tyr_D$) was used to eliminate the $Tyr_D^{\bullet+}$ signal, which would otherwise dominate the PSII EPR spectrum in the radical region (32). At each potential dark spectra and spectra after illumination at 77 K were recorded. Figure 2A shows a scan of the radical region around g=2. The appearance and disappearance of the EPR signal as a function of potential can be observed. This signal has been assigned to the low-field edge of the ground state doublet of the semiquinone, $Q_B^{\bullet-}Fe^{2+}$ (29).

Figure 2B shows a full spectrum scan of the same samples as used in Figure 2A after illumination at 77 K. A peak at 4000 gauss (g=1.66) shows a potential dependence similar to that of the $Q_B^{\bullet-}Fe^{2+}$ signal. The g=1.66 signal has been assigned to the $Q_A^{\bullet-}Fe^{2+}Q_B^{\bullet-}$ biradical state (30, 31). The low temperature illumination generates $Q_A^{\bullet-}$ in nearly all of the centers. No electron transfer occurs from $Q_A^{\bullet-}$ to $Q_B$ or to $Q_B^{\bullet-}$ at 77 K (31), therefore the biradical signal should only be observed if $Q_B^{\bullet-}$ were present before the 77 K illumination. Thus the biradical signal can be used to monitor the presence of $Q_B^{\bullet-}$ independently of the $Q_B^{\bullet-}Fe^{2+}$ signal.

To assess the proportion of $Q_B^{\bullet-}$ formed during the titration, the signal size of the $Q_B^{\bullet-}Fe^{2+}$ signal if present in 100% of the centers was estimated. In a dark-adapted sample $Q_B^{\bullet-}$ is present in ~40% of the centers, while $Q_B$ is present in the rest (3, 31, 33). That proportion can be inverted by illuminating at 77 K and subsequently thawing in darkness (3). Therefore the sum of the amplitudes of the signals present before and after this treatment should yield the size of the signal when $Q_B^{\bullet-}$ is present in all of the centers. This experiment was done and the estimated value for 100% $Q_B^{\bullet-}$ was used to calibrate the amplitudes of the EPR signals in the titrations.

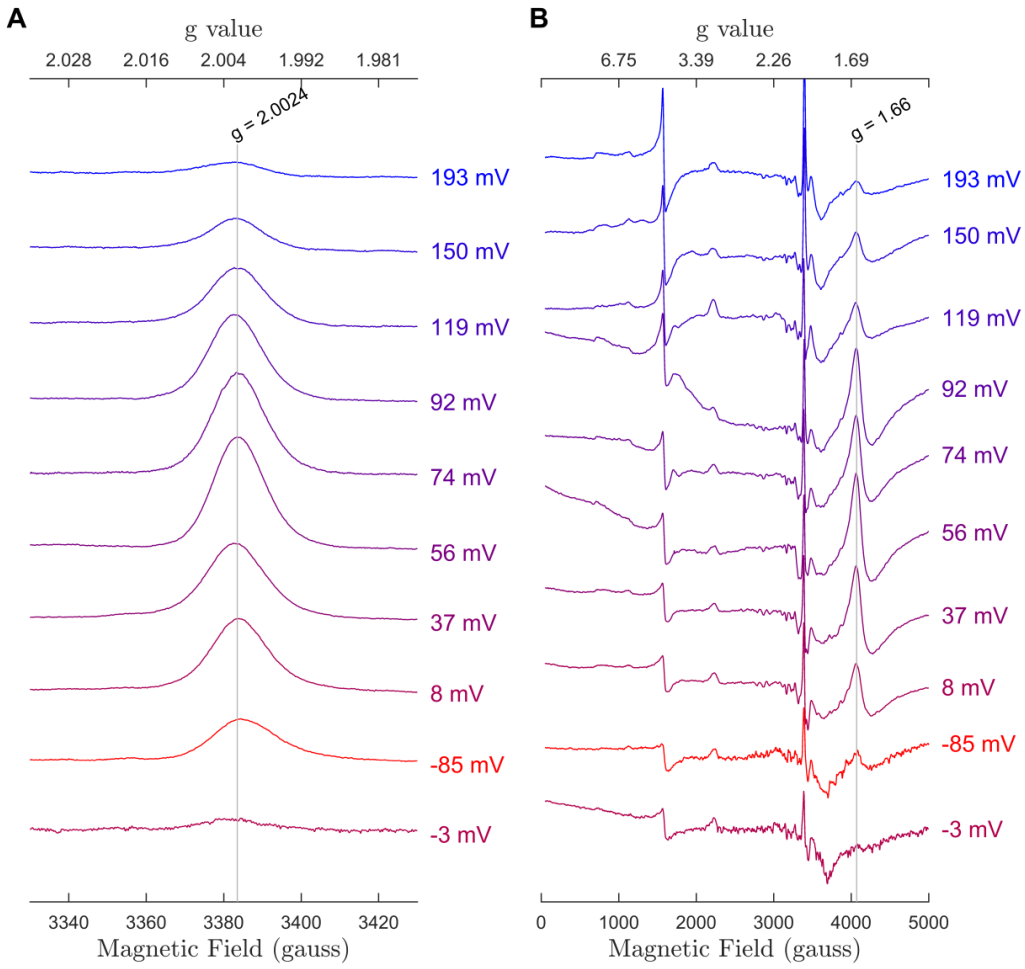


Figure 2: EPR spectra of PSII poised at different potentials. A: Radical region spectra showing the $Q_B^{\bullet-}Fe^{2+}$ at g=2.0024 (microwave power: 205.1 mW; modulation amplitude 10.53 gauss). B: Wider scan of the same samples after 77 K illumination showing the $Q_A^{\bullet-}Fe^{2+}Q_B^{\bullet-}$ signal at g=1.66. (microwave power: 20 mW, modulation amplitude: 25.35 gauss)

Figure 3 shows a plot of the normalized $Q_B^{\bullet-}Fe^{2+}$ and $Q_A^{\bullet-}Fe^{2+}Q_B^{\bullet-}$ signals versus the measured potential, combining data from three individual titrations. Titrations were carried out in oxidizing and reducing directions. The maximum amplitude, at 67 mV, represented about 55% of the centers in the

stable $Q_B^{\bullet-}$ state. Data were fitted using the model first established by Michaelis (34). The resulting potentials for the two couples were $E_m(Q_B/Q_B^{\bullet-})$ = 92 ± 36 mV and $E_m(Q_B^{\bullet-}/Q_BH_2)$ = 43 ± 36 mV.

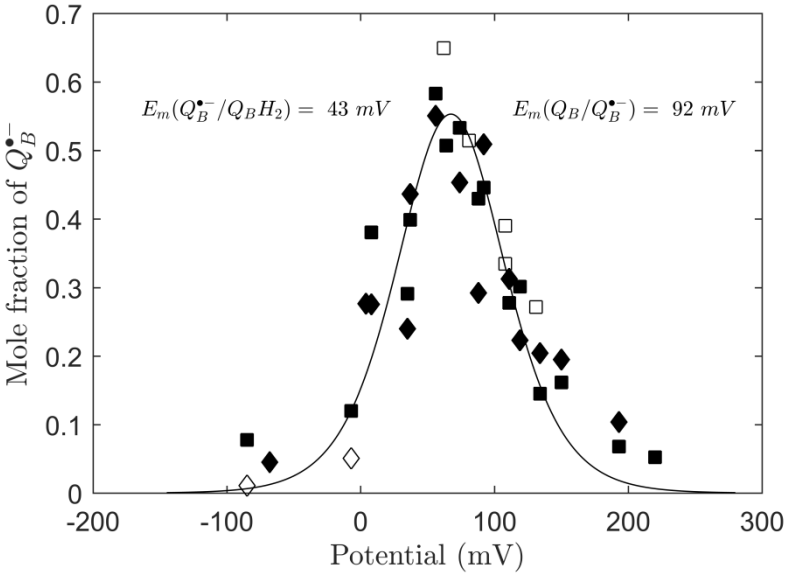


Figure 3: Titration of the $Q_B^{\bullet-}$ semiquinone using two different EPR signals. Open squares: oxidizing titration of the $Q_B^{\bullet-}Fe^{2+}$ signal; closed squares: reducing titration of the $Q_B^{\bullet-}Fe^{2+}$ signal; closed diamonds: reducing titration of the $Q_A^{\bullet-}Fe^{2+}Q_B^{\bullet-}$ signal; open diamonds: oxidizing titration of the $Q^{\bullet-}Fe^{2+}Q_B^{\bullet-}$ signal.

The retention of the $Mn_4O_5Ca$ cluster during the course of the titration was assessed in two ways: firstly by the presence of free "hexaquo" $Mn^{2+}$ signals in the spectra, representing a loss of the $Mn_4O_5Ca$ cluster and secondly by the ability to form the $S_2$ multiline signal (35). Before adding redox mediators, no free $Mn^{2+}$ was observed. After the addition of redox mediators and equilibration in the dark, a small amount of free $Mn^{2+}$ was detected. This could arise from centres that had lost the extrinsic polypeptides at the luminal side of PSII during the purification and were thus more susceptible to reduction. The size of the free $Mn^{2+}$ signals did not increase during the redox titrations. Further evidence that the manganese cluster was retained in most centers was the ability to generate the $S_2$ multiline signal by illumination at 200 K. Illumination at this temperature has been shown to oxidize the $Mn_4O_5Ca$ cluster from $S_1$ to $S_2$ but not to higher S-states (36). This is taken as an indication that the majority of the centres did not lose the $Mn_4O_5Ca$ cluster during the course of the titration. Although the intensity of the multiline signal decreased at the lowest potentials, it partially recovered again at higher potentials (see Figure S1). The fact that the recovery is only partial is likely due to a fraction of the centers in the $S_1$ state being reduced to $S_0$ at the lowest potentials.

In addition to the redox titrations of the EPR signals associated with $Q_B^{\bullet-}$, pH-dependent thermoluminescence measurements were used to determine the difference in redox potential between

the $Q_A/Q_A^{\bullet-}$ and $Q_B/Q_B^{\bullet-}$ couples. Thermoluminescence measures the emission of luminescence associated with the heating-induced back-reaction of a stable charge-separated state. The peak temperature of thermoluminescence is indicative of the energy stored in the charge-separated state and is determined by redox potentials of both the recombination partners, in this case $S_2/S_1$ and $Q_B/Q_B^{\bullet-}$ (3, 23). The $S_2/S_1$ couple does not involve protonation and is therefore independent of pH (37). The $Q_B/Q_B^{\bullet-}$ couple involves proton release when $Q_B^{\bullet-}$ is re–oxidized and is expected to follow Nernst behaviour (20, 38) with the redox potential changing by −59 mV per pH–unit. Thus the pH dependence of the $S_2Q_B^{\bullet-}$ recombination peak position should reflect this process and can be used as an empirical calibration of the change in emission temperature in terms of the change in the redox potential of $Q_B$.

Figure 4 shows the thermoluminescence curves of long dark–adapted PSII samples after one saturating flash at different pH–values. A clear shift of the peak positions to lower temperatures with increasing pH can be seen. The insert in Figure 4 shows a plot of peak temperature versus the pH, from which a linear dependence of −11.9 °C per pH–unit can be observed. Using the ΔE relationship given by the Nernst equation, this translates to −4.95 meV $°C^{-1}$. A similar slope was observed by Vass and Inoue (39) in their study of the pH–dependence of thermoluminescence.

This calibration was then used to estimate the gap between the $Q_A$ and $Q_B$ couples. Figure 4 (red curve) shows the $S_2Q_A^{\bullet-}$ recombination band at pH 7 in the presence of DCMU occurring at 14 °C. The difference in peak positions of 36 °C between the $S_2Q_A^{\bullet-}$ and $S_2Q_B^{\bullet-}$ peaks corresponds to an energy gap of 178 meV. Given a potential for $Q_A/Q_A^{\bullet-}$ of −144 mV and taking into account the upshift caused by the binding of DCMU of ~52 mV (40), this would result in a potential of ~86 mV for the $Q_B/Q_B^{\bullet-}$ couple, close to the value reported here from the equilibrium redox titrations.

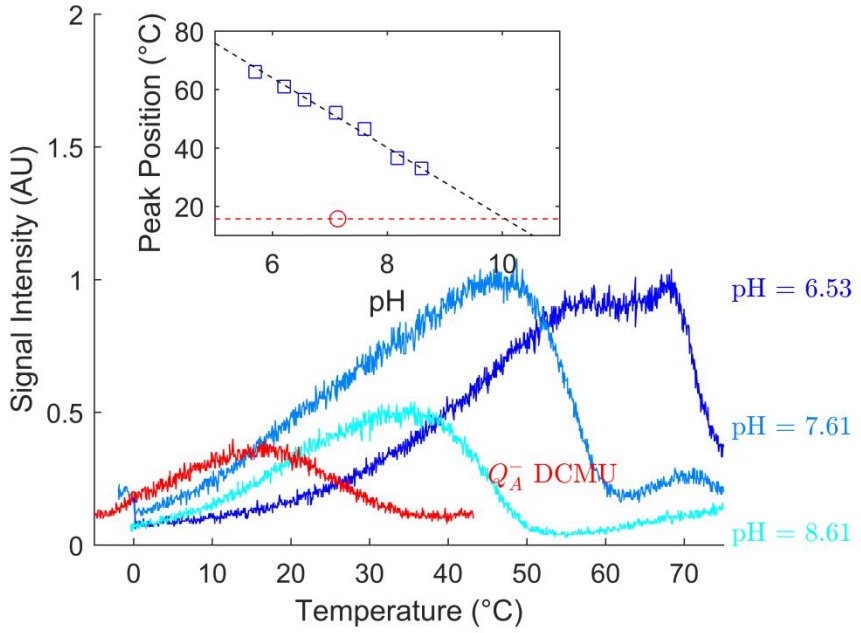


Figure 4: Thermoluminescence of long-dark-adapted PSII cores from *T. elongatus*. Blue: after one saturating flash at different values of pH. Red: after the addition of DCMU at pH 7. The insert shows a plot of the $S_2Q_B^{\bullet-}$ peak position versus the pH. At pH 6.5 a TL band ~70°C becomes the dominant emission but is not attributed to the $S_2Q_B^{\bullet-}$, it is more likely to be from the so-called C-band which has been attributed to $Tyr_D^{\bullet}Q_A^{\bullet-}$ recombination (41).

## Discussion

In the present work, the midpoint potential of the terminal electron acceptor of PSII, $Q_B$, was measured with EPR. The results show that the semiquinone, $Q_B^{\bullet-}$, is thermodynamically stable at pH 7. The redox potentials derived from the data for the two redox couples are $E_m(Q_B/Q_B^{\bullet-}) \approx 90$ mV and $E_m(Q_B^{\bullet-}/Q_BH_2) \approx 40$ mV. In addition, we have estimated the difference in redox potentials between the $Q_A/Q_A^{\bullet-}$ and $Q_B/Q_B^{\bullet-}$ couples using the pH–dependence of $S_2Q_A^{\bullet-}$ and $S_2Q_B^{\bullet-}$ recombination measured by thermoluminescence. The energy difference obtained from this approach is ~230 meV, This value is similar to the difference between the $E_m$ = -144mV for $Q_A/Q_A^{\bullet-}$ (15, 16) and +90 mV for $Q_B/Q_B^{\bullet-}$ presented here.

The following aspects are discussed below: i) the stabilisation of the semiquinone state; ii) the preferential binding of the quinone over the quinol in the $Q_B$ site; and iii) the difference in redox potential between $Q_A$ and $Q_B$. In addition, as the results markedly contradict a recent publication (25), these discrepancies are also addressed and a potential explanation is provided.

## Stabilisation of the semiquinone state within the $Q_B$ site

A fit of the Nernst model to our data shows the difference between the $Q_B/Q_B^{\bullet-}$ and $Q_B^{\bullet-}/Q_BH_2$ couples, $\Delta E_m$, to be ~ +50 mV, a value that agrees with the measured maximum of ~55% of stable $Q_B^{\bullet-}$ in the EPR signal generated in the titrations. This $\Delta E_m$ is indicative of the degree of stabilisation of the semiquinone radical, $Q_B^{\bullet-}$, in the site. When titrating a free quinone, the semiquinone is not stabilized, the redox transition occurs as a steeper n=2 curve, typical of a two–electron transition, no intermediate semiquinone can be observed and the $\Delta E_m$ is negative ($\Delta E_m$ <<−500 mV). Our data indicate that $Q_B^{\bullet-}$ is strongly bound and therefore stabilized by the $Q_B$ site. The structure of the $Q_B$ site (Fig 1) shows several features that likely contribute to the relative stability of $Q_B^{\bullet-}$ including: i) the proximity to the non–heme ferrous iron; ii) hydrogen bonds from to both carbonyls of the quinone; and iii) the likely protonation of the distal H–bonding D1Ser264/His252 pair (4).

This strong stabilisation can be rationalized in part as a damage–prevention mechanism. In PSII, back–reactions from $P^{\bullet+}Q_A^{\bullet-}$ result in damage to the complex (9, 16). A large gap between the $Q_A/Q_A^{\bullet-}$ and $Q_B/Q_B^{\bullet-}$ couples would favor $Q_B$ reduction and lower the equilibrium concentration of $Q_A^{\bullet-}$, thereby diminishing the likelihood of a damaging back-reaction from $Q_A^{\bullet-}$. It would, therefore, be beneficial to stabilize the semiquinone to a point where the $Q_B/Q_B^{\bullet-}$ couple is more oxidizing than the $Q_B^{\bullet-}/Q_BH_2$ couple.

This stabilisation of the semiquinone would come at a cost because a more positive $E_m(Q_B/Q_B^{\bullet-})$ must yield a more negative $E_m(Q_B^{\bullet-}/Q_BH_2)$ in order to maintain the chemical requirement that the average $E_m$ for the two couples remains unchanged. Back–reactions from the fully reduced quinol $Q_BH_2$ to $Q_A$ would therefore become more likely. These back–reactions would only occur when the plastoquinone pool is reduced because quinol/quinone exchange occurs orders of magnitude faster (≈10 ms, (42)) than the $S_2Q_BH_2$ back-reaction, which is predicted to decay with kinetics between the recombination rates of $Q_A^{\bullet-}$ and $Q_B^{\bullet-}$ with $S_2$ (i.e. between ~1 s and ~30 s (43)).

The high potential $E_m$ (~90mV) for the $Q_B/Q_B^{\bullet-}$ also means that $Q_B^{\bullet-}$ is a poor reductant for $O_2$ forming superoxide ($E_m(O_2/O_2^{\bullet-}) \approx$ -160mV). It has been suggested that $Q_B^{\bullet-}$ may be a source of reactive oxygen species (44), however, its very long lifetime, with half-times of hours in the presence of $S_1$ and $S_0$ (3, 31, 33), has argued against this. The present work showing the thermodynamic stabilisation of $Q_B^{\bullet-}$ provides a good explanation for its lack of reactivity with oxygen and for its very long lifetime in the dark.

The presence of a stabilised $Q_B^{\bullet-}$ directly contradicts a recent report (22) (discussed in detail below) but is not without precedence. A reductive titration of the g=1.66 biradical signal with PSII particles from *Phormidium laminosum* was reported previously as part of the early work done to

identify the origin of the signal (30). Although no reversibility was demonstrated and the signal size was not quantified, a thermodynamically stable $Q_B^{\bullet-}$, similar to that reported in this work, was clearly present in the reductive titration.

A thermodynamically stable $Q_B^{\bullet-}$ was also present in the homologous purple bacterial reaction centers from *Rhodobacter sphaeroides* (26), *Chromatium vinosum* (27) and *Bastochloris viridis* (28). These titrations, which have been replotted and refitted here (supplementary material) show ~30–50% of the total quinone form as a stable semiquinone. The exact $\Delta E_m$ and $E_m^{avrg}$ all differ from each other to some extent, perhaps reflecting different mechanistic requirements in the different species, but in all reaction centers, the semiquinone, $Q_B^{\bullet-}$, is clearly thermodynamically stable. Together, these studies in the literature (26–28, 30) provide strong support for the current results.

## Preferential binding of the quinone vs the quinol

Although the redox potential of the plastoquinone in the pool from *T. elongatus* has not been measured, it is expected to be very similar to that in other organisms, i.e. a two–electron transition at 117 mV (45, 46). The average for the two $Q_B$ redox couples measured here ($E_m^{avrg} \approx 67$ mV) is therefore about 50 mV lower than that of the plastoquinone pool. This represents a significant driving force for the release of the $PQH_2$ to the pool. This should be considered as an additional energy loss in the on–going effort to understand energy use in PSII.

From the difference in redox potential, the ratio of the binding constants for the quinone and the quinol forms can be calculated (16, 47). It is found that the quinone is bound to the $Q_B$ site about 60 times more tightly than the quinol. Since PSII is a water-plastoquinone photo-oxidoreductase, it seems appropriate that the binding of the substrate (the quinone) is favoured over that of the product (the quinol). This preferential binding of the quinone would allow PSII to function better under conditions where the pool is significantly reduced. Also this would be beneficial in terms of the stabilisation of the $Q_B/Q_B^{\bullet-}$ couple in relation to the $Q_B^{\bullet-}/Q_BH_2$ couple, as discussed above.

In the literature it has often been assumed that the binding constants of the quinone and quinol in the $Q_B$ site are equal both in PSII and in purple bacterial reaction centers (e.g. (19, 21)). Nevertheless, the $Q_B^{\bullet-}$ redox titrations in purple bacterial reaction centers clearly indicated the preferential binding of the quinone over the quinol (26) and other reports favour this binding regime (6, 48) at least in part because it seemed mechanistically more likely. The experimental findings in the present work indicate preferential binding of the quinone over the quinol.

## The difference in redox potentials between $Q_A$ and $Q_B$

The difference in redox potentials between the $Q_A/Q_A^{\bullet-}$ and $Q_B/Q_B^{\bullet-}$ couples reported here (~230 meV) is larger than previously estimated (70–80 meV) (23, 43). The earlier estimates of the energy gap between $Q_A$ and $Q_B$ were based on estimates of the equilibrium constant that were

obtained from the kinetics of the forward and backward electron transfer reactions between $Q_A$ and $Q_B$ (18–20, 43, 49, 50).

A difference between equilibrium redox potential studies and those based on kinetic estimates is that redox titrations require equilibration over a long period while the kinetic estimates represent a range of dynamic states. It has been demonstrated experimentally that the driving force (energy gap) for the $Q_A^{\bullet-}$ to $Q_B$ step in the purple bacterial reaction centers does not control the kinetics (51, 52). Instead the rate-limiting step is determined by a gating process; i.e. protein and/or cofactor movements associated with the proton-coupled electron transfer (51–53). In PSII several reports indicate a similar situation (31, 54, 55) and similar gating is assumed to be present (4, 7, 8, 31, 54, 55). This could compromise estimates of the energy gap from kinetic measurements.

Furthermore redox titrations of multi-cofactor proteins imply that the titration of lower potential components must be done in the presence of the reduced form of the, often adjacent, higher potential components. This can result in a shift in the potential of the lower potential component(s) compared to functional conditions. In this case, $Q_B$ is the highest potential component in the complex, so it will not be influenced by any higher potential components. In contrast, $Q_A$ will inevitably be titrated in the presence of $Q_BH_2$, whilst in functional conditions $Q_A$ is reduced with $Q_B$ present. To explain the difference between the energy gaps based on kinetic measurements compared to those based on equilibrium redox titrations, the binding of $Q_BH_2$ would have to shift the $E_m$ of $Q_A/Q_A^{\bullet-}$ by ~ -150 mV. It is known that binding of herbicides in the $Q_B$ site can shift the $E_m(Q_A/Q_A^{\bullet-})$ by ~50mV (56) and a change in the charge on the adjacent $Fe^{2+}$ by binding of bicarbonate results in a -74 mV shift in the $E_m(Q_A/Q_A^{\bullet-})$ (16). While an effect of $Q_BH_2$ binding on the $E_m$ of $Q_A/Q_A^{\bullet-}$ cannot be ruled out, it seems unlikely that it is responsible for such a large effect.

Here we made an independent estimate of the energy gap between $Q_A/Q_A^{\bullet-}$ and $Q_B/Q_B^{\bullet-}$ by estimating empirically the energy gap between $S_2Q_A^{\bullet-}$ and $S_2Q_B^{\bullet-}$ as a function of pH. It was assumed that the energy gap determining the peak position of the thermoluminescence will follow Nernst behaviour and shift by 59meV per pH unit. The resulting value (~130meV) is similar to the energy gap obtained from the equilibrium redox titrations (~134meV). We remain sceptical over the closeness of these two approximations but it allows us to propose that this energy gap may be correct. Indeed a large energy gap would make sense in functional terms. As $Q_B^{\bullet-}$ is the terminal electron acceptor, it cannot be prevented from back-reacting by "kinetic control", i.e. by making sure it undergoes forward electron transfer before it back-reacts (9). Thus wasteful and damaging back-reactions can be minimised by increasing the energy gap between the $Q_A/Q_A^{\bullet-}$ and $Q_B/Q_B^{\bullet-}$ couples.

## Rationalizing the conflicting report in the literature

The findings in the present work differ significantly from a recently published study on the redox potentials of $Q_B$ (25). In that work, redox titrations were performed in which the ability to form $Q_B^{\bullet-}$ by a single saturating flash was monitored by FTIR measurements in a spectroelectrochemical thin cell (25). Although this is not a direct measurement of $Q_B^{\bullet-}$, but rather a measurement of the ability to form $Q_B^{\bullet-}$ upon flash illumination (or in principle to form $Q_BH_2$ if $Q_B^{\bullet-}$ were already present), this method should in principle be usable for a $Q_B$ titration. Their results, however, showed no evidence for stable $Q_B^{\bullet-}$ formation, instead a redox curve was reported that was essentially indistinguishable from an n=2 curve, with an $E_m$ = 155 mV at pH 6.5 (equivalent to 125 mV at pH 7). The $E_m$ and the n=2 curve are both characteristic of a titration of free plastoquinone. While the PSII cores have no membrane and thus no membrane-localised quinone pool, they do contain one or two free quinones in addition to $Q_B$ and these quinones act as a limited plastoquinone pool (31, 57).

In the present work we show that the potential of the quinone in the $Q_B$ site is more negative than that of free quinone; therefore in a reductive titration the free quinone will be reduced before the $Q_B$ quinone. The free quinol will equilibrate with, and eventually occupy the $Q_B$ site. If the mediation with the $Q_B$ site is poor, i.e. the mediators are at inappropriate redox potentials or have restricted access to the $Q_B$ site, electrons cannot be removed from $Q_BH_2$ and it will remain present in the site irrespective of the potential of the $Q_B^{\bullet-}/Q_BH_2$ couple. In such a case, the loss of the ability to form $Q_B^{\bullet-}$ with a flash would reflect the potential of the free quinone, with an n=2 Nernst dependency. Given that only three mediators were used in the titration (25), out of which only one was in the appropriate range (1-methoxy-5-methylphanazinium methosulfate, Em =+63 mV), it seems likely that because of insufficient redox mediation, the potential of free plastoquinone was measured in the work of Kato et al. (25). The slight shift from the literature value for the pool quinone, if significant, might be attributed to the environment of the free quinone within the cavities, lipids and detergent of the isolated PSII core complex, which is likely to be slightly different to that of quinone in the lipid membrane.

The weaker binding of $PQH_2$ compared to PQ reported in the present work may mean that it would not fully occupy the $Q_B$ site and it would have a tendency to leave the site vacant. This would exacerbate a poor mediation problem as any formation of $Q_B^{\bullet-}$ would require the oxidised mediator to encounter $Q_BH_2$ in the site.

## Conclusion

Figure 5 summarizes the results of the present work and provides a consistent energetic description of PSII, now including the two redox potentials of the $Q_B$ couples. This provides insights into the redox tuning of $Q_B$ with respect to the redox potentials of its neighbouring redox partners, $Q_A$ and free plastoquinone. The energy gap between the $Q_A/Q_A^{\bullet-}$ and the two $Q_B$ redox couples reported here is

significantly larger than previously assumed. The redox potentials need to be high enough compared to that of $Q_A$ to provide for sufficient driving force and to minimize back-reactions. The redox potential of the plastoquinone pool limits the average value of the two $Q_B$ couples. However the measured value shows that in PSII ~50 meV of driving force is expended to ensure rapid de-binding of the quinol and the preferential binding of the quinone. These data indicate that the protein tunes the thermodynamics of the $Q_B$ redox chemistry to optimise function over a wide range of plastoquinone pool reduction states while minimising back-reactions and side reactions with $O_2$.

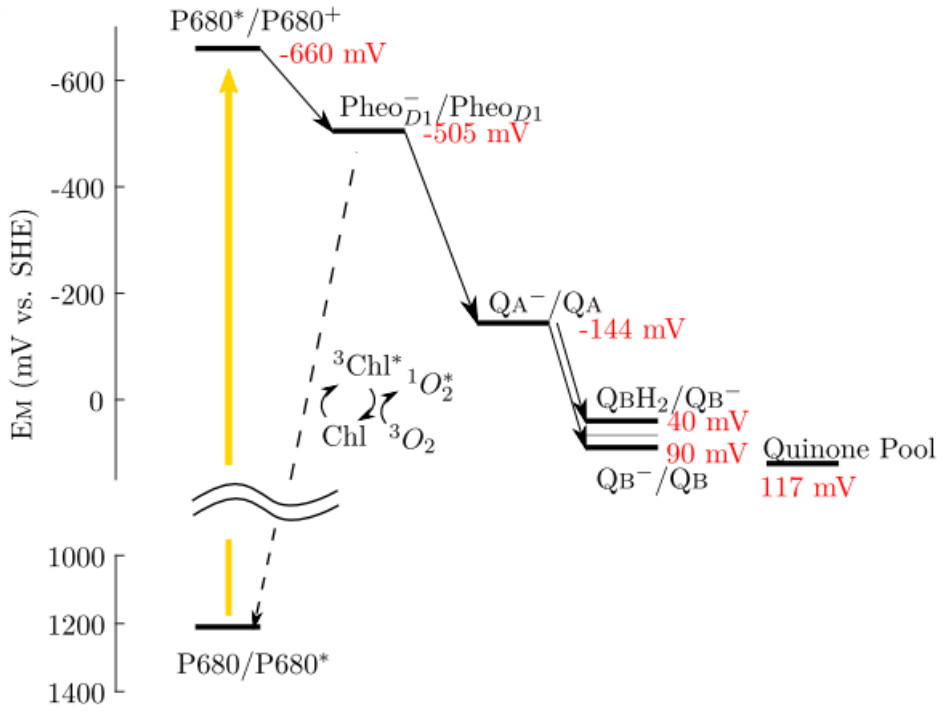


Figure 5: Redox scheme of PSII. Redox potentials values were taken from the present work for the $Q_B$ couples and from (16) for $Q_A$ , from (58) for $Pheo_{D1,}$ from (2) for P680 and from (45, 46) for PQ.

## Materials and Methods

*Isolation of PSII from T. elongatus* – PSII cores were isolated from (D2-Y160F; CP43-His strain (59)) using a method based on that of Sugiura and Inoue (60) with specific modifications described in the SI.

*EPR-detected potentiometric titrations* - Multiple PSII preparations were pooled to yield 7-10 ml of purified PSII at 0.7 mg(Chl) $ml^{-1}$ in titration buffer. Redox titrations were carried out essentially as described by Dutton (61) at 15 °C under a bicarbonate-enriched argon atmosphere in absolute

darkness and in the presence of the following redox mediators at 50 µM: *N,N,N′,N′*-tetramethyl-*p*-phenylenediamine (300 mV), 2,6-Dichlorophenolindophenol (217 mV), Phenazine methosulfate (80 mV), Thionine (64 mV), Phenazine ethosulfate (55 mV), Methylene blue (11 mV), Pyocyanin (−34 mV), Indigotetrasulfonate (−46 mV), Resorufin (−51 mV). Reductive titrations were carried out using sodium dithionite, oxidative titrations were carried out using potassium ferricyanide. EPR spectra were recorded on a Bruker ElexSys X-band spectrometer fitted with an Oxford Instruments liquid helium cryostat and temperature control system. Illumination at 77 K was carried out in an un-silvered dewar with a halogen lamp (LQ 2600, Fiberoptic-Heim AG, CH). Each sample was illuminated for 20 min.

*Thermoluminescence* - Measurements were carried out using a lab-built apparatus (62). PSII core complexes were suspended in buffer 1 (MOPS was used instead of MES at pH >7 and HEPES at pH >8, 20% glycerol instead of 10%) at a concentration of 20 µg(Chl) $ml^{-1}$. Samples were dark-adapted for >1 h at 4 °C, 200 µl samples were loaded in absolute darkness and if required, DCMU (dissolved in ethanol) was added to the sample on the sample plate (50 µM final concentration). Excitation flashes were provided at 4 °C by the second harmonic of a Nd-YAG laser (Minilite II, Continuum, CA, USA), using ~5 ns pulses at 532 nm and then rapidly chilled (<30 s) to 253 K with liquid $N_2$. The frozen samples were then heated at a constant rate of 20 °C $min^{-1}$ and TL emission was detected with a photomultiplier (H7422-50, Hamamatsu, Japan). The signal was amplified using a transimpedance amplifier (C7319, Hamamatsu, Japan) and digitized using a microcontroller board based on the Atmel SAM3X8E ARM Cortex-M3 CPU (Arduino Due).


## Acknowledgements:

The authors are grateful for access to the EPR facilities available at the Aix-Marseille University EPR center and at the national TGE-RPE network (FR3443). This work was supported by the Royal Society Wolfson Research Merit Award to AWR and by Biotechnology and Biological Sciences Research Council (BBSRC) grants BB/K002627/1 and BB/R00921X/ to AWR. These BBSRC grants also supported AF and SDC. SDC was also supported by an Imperial College London Scholarship during his PhD studies. J.D. was supported by EPSRC Standard Research Studentship (DTG) EP/P504953/1 from the Energy Futures Laboratory of Imperial College.


## References


1. Dau H, Zaharieva I (2009) Principles, efficiency, and blueprint character of solar-energy conversion in photosynthetic water oxidation. *Acc Chem Res* 42(12):1861–1870.

2. Rappaport F, Diner BA (2008) Primary photochemistry and energetics leading to the oxidation of the (Mn)4Ca cluster and to the evolution of molecular oxygen in Photosystem II. *Coord Chem Rev* 252(3–4):259–272.

3. Rutherford AW, Crofts AR, Inoue Y (1982) Thermoluminescence as a probe of Photosystem II photochemistry. The origin of the flash-induced glow peaks. *Biochim Biophys Acta* 682(3):457–465.

4. Saito K, Rutherford AW, Ishikita H (2013) Mechanism of proton-coupled quinone reduction in Photosystem II. *Proc Natl Acad Sci USA* 110(3):954–959.

5. Wraight CA (2004) Proton and electron transfer in the acceptor quinone complex of photosynthetic reaction centers from *Rhodobacter sphaeroides*. *Front Biosci* 9(1–3):309–337.

6. Wraight CA (1981) Oxidation-reduction physical chemistry of the acceptor quinone complex in bacterial photosynthetic reaction centers: evidence for a new model of herbicide activity. *Isr J Chem* 21(4):348–354.

7. Müh F, Glöckner C, Hellmich J, Zouni A (2012) Light-induced quinone reduction in photosystem II. *Biochim Biophys Acta* 1817(1):44–65.

8. Cardona T, Sedoud A, Cox N, Rutherford AW (2012) Charge separation in photosystem II: a comparative and evolutionary overview. *Biochim Biophys Acta* 1817(1):26–43.

9. Rutherford AW, Osyczka A, Rappaport F (2012) Back-reactions, short-circuits, leaks and other energy wasteful reactions in biological electron transfer: Redox tuning to survive life in O2. *FEBS Lett* 586(5):603–616.

10. Johnson GN, Rutherford AW, Krieger A (1995) A change in the midpoint potential of the quinone QA in Photosystem II associated with photoactivation of oxygen evolution. *Biochim Biophys Acta* 1229(2):202–207.

11. Rutherford AW, Paterson DR, Mullet JE (1981) A light-induced spin-polarized triplet detected by EPR in Photosystem II reaction centers. *Biochim Biophys Acta* 635(2):205–214.

12. Durrant JR, Giorgi LB, Barber J, Klug DR, Porter G (1990) Characterisation of triplet states in isolated Photosystem II reaction centres: Oxygen quenching as a mechanism for photodamage. *Biochim Biophys Acta* 1017(2):167–175.

13. Krieger A, Rutherford AW, Johnson GN (1995) On the determination of redox midpoint potential of the primary quinone electron acceptor, QA, in Photosystem II. *Biochim Biophys Acta* 1229(2):193–201.

14. Krieger A, Weis E, Demeter S (1993) Low-pH-induced Ca2+ion release in the water-splitting system is accompanied by a shift in the midpoint redox potential of the primary quinone acceptor QA. *Biochim Biophys Acta* 1144(3):411–418.

15. Shibamoto T, Kato Y, Sugiura M, Watanabe T (2009) Redox potential of the primary plastoquinone electron acceptor QA in photosystem II from Thermosynechococcus elongatus determined by spectroelectrochemistry. *Biochemistry* 48(45):10682–10684.

16. Brinkert K, De Causmaecker S, Krieger-Liszkay A, Fantuzzi A, Rutherford AW (2016) Bicarbonate-induced redox tuning in Photosystem II for regulation and protection. *Proc Natl Acad Sci USA* 113(43):12144–12149.

17. Umena Y, Kawakami K, Shen J-R, Kamiya N (2011) Crystal structure of oxygen-evolving photosystem II at a resolution of 1.9 Å. *Nature* 473(7345):55–60.

18. Diner BA (1977) Dependence of the deactivation reactions of Photosystem II on the redox state of plastoquinone pool a varied under anaerobic conditions. Equilibria on the acceptor side of Photosystem II. *Biochim Biophys Acta* 460(2):247–258.

19. Bouges-Bocquet B (1975) Electron Acceptors of Photosystem II. *Proceedings of the 3rd International Congress on Photosynthesis*, ed Avron M (Elsevier), pp 579–588,.

20. Robinson HH, Crofts AR (1984) Kinetics of proton uptake and the oxidation-reduction reactions of the quinone acceptor complex of PS II from pea chloroplasts. *Proc. Intrntl. Cong. Photosynth. Vol I. Brussels, Belgium, Aug 1-6, 1983*, ed Sybesma C (Martinus Nijhoff/Dr. W. Junk, The Hague), pp 477–480.

21. Crofts AR, Wraight CA (1983) The electrochemical domain of photosynthesis. *Biochim Biophys Acta* 726(3):149–185.

22. Rappaport F, Cuni A, Xiong L, Sayre RT, Lavergne J (2005) Charge recombination and thermoluminescence in photosystem II. *Biophys J* 88(3):1948–58.

23. Rappaport F, Lavergne J (2009) Thermoluminescence: theory. *Photosynth Res* 101(2–3):205–216.

24. Rose S, et al. (2008) D1-arginine257 mutants (R257E, K, and Q) of *Chlamydomonas reinhardtii* have a lowered $Q_B$ redox potential: Analysis of thermoluminescence and fluorescence measurements. *Photosynth Res* 98(1–3):449–468.

25. Kato Y, Nagao R, Noguchi T (2016) Redox potential of the terminal quinone electron acceptor $Q_B$ in photosystem II reveals the mechanism of electron transfer regulation. *Proc Natl Acad Sci USA* 113(3):620–625.

26. Rutherford AW, Evans MCW (1980) Direct measurement of the redox potential of the primary and secondary quinone electron acceptors in Rhodopseudomonas sphaeroides (wild-type) by EPR Spectrometry. *FEBS Lett* 110(2):257–261.

27. Heathcote P, Rutherford AW (1986) An EPR Signal Arising from QB-Fe in *Chromatium vinosum*. *Progress in Photosynthesis Research Vol.1* (Dordrecht), pp 201–204.

28. Rutherford AW, Heathcote P, Evans MCW (1979) Electron-paramagnetic-resonance measurements of the electron-transfer components of the reaction centre of *Rhodopseudomonas viridis*. Oxidation--reduction potentials and interactions of the electron acceptors. *Biochem J* 182(2):515–523.

29. Sedoud A, et al. (2011) Semiquinone-iron complex of Photosystem II: EPR signals assigned to the low-field edge of the ground state doublet of $Q_A^{\bullet-}Fe^{2+}$ and $Q_B^{\bullet-}Fe^{2+}$. *Biochemistry* 50(27):6012–6021.

30. Corrie AR, Nugent JHA, Evans MCW (1991) Identification of EPR signals from the states QaQb and Qb in photosystem II from *Phormidium laminosum*. *Biochim Biophys Acta* 1057(3):384–390.

31. Fufezan C, Zhang C, Krieger-Liszkay A, Rutherford AW (2005) Secondary quinone in photosystem II of *Thermosynechococcus elongatus*: Semiquinone-iron EPR signals and temperature dependence of electron transfer. *Biochemistry* 44(38):12780–12789.

32. Sugiura M, et al. (2004) Site-directed mutagenesis of *Thermosynechococcus elongatus* Photosystem II: the $O_2$-evolving enzyme lacking the redox-active Tyrosine D. *Biochemistry* 43:13549–13563.

33. Wollman FA (1978) Determination and modification of the redox state of the secondary acceptor of Photosystem II in the dark. *Biochim Biophys Acta* 503(2):263–273.

34. Michaelis L (1932) Theroy of the reversible two-step oxidation. *J Biol Chem* 96(3):703–715.

35. Dismukes GC, Siderer Y (1980) EPR spectroscopic observations of a manganese center associated with water oxidation in spinach chloroplasts. *FEBS Lett* 121(1):78–80.

36. Brudvig GW, Casey JL, Sauer K (1983) The effect of temperature on the formation and decay of the multiline EPR signal species associated with photosynthetic oxygen evolution. *Biochim Biophys Acta* 723(3):366–371.

37. Klauss A, Haumann M, Dau H (2012) Alternating electron and proton transfer steps in photosynthetic water oxidation. *Proc Natl Acad Sci USA*. 109*:*16035–16040.

38. Rutherford AW, Renger G, Koike H, Inoue Y (1984) Thermoluminescence as a probe of photosystem II. The redox and protonation states of the secondary acceptor quinone and the O2-evolving enzyme. *Biochim Biophys Acta* 767(3):548–556.

39. Vass I, Inoue Y (1986) pH dependent stabilization of S2QA- and S2QB- charge pairs studied by thermoluminescence. *Photosynth Res* 10(3):431–436.

40. Krieger-Liszkay A, Rutherford AW (1998) Influence of herbicide binding on the redox potential of the quinone acceptor in photosystem II: relevance to photodamage and phytotoxicity. *Biochemistry* 37(50):17339–44.

41. Johnson GN, Boussac A, Rutherford AW (1994) The origin of 40-50°C thermoluminescence bands in Photosystem II. *Biochim Biophys Acta* 1184(1):85–92.

42. De Wijn R, Van Gorkom HJ (2001) Kinetics of electron transfer from QA to QB in photosystem II. *Biochemistry* 40(39):11912–11922.

43. Petrouleas V, Crofts AR (2005) The iron-quinone acceptor complex. *Photosystem II* ed. Wydrzynski TJ, Satoh K, Freeman JA (Springer-Verlag, Berlin/Heidelberg), pp 177–206.

44. Pospíšil P (2012) Molecular mechanisms of production and scavenging of reactive oxygen species by photosystem II. *Biochim Biophys Acta* 1817(1):218–231.

45. Golbeck JH, Kok B (1979) Redox titration of electron acceptor Q and the plastoquinone pool in Photosystem II. *Biochim Biophys Acta* 547(2):347–360.

46. Rich PR, Bendall DS (1980) The kinetics and thermodynamics of the reduction of cytochrome c by substituted p-benzoquinols in solution. *Biochim Biophys Acta* 592(3):506–518.

47. Zhu Z, Gunner MR (2005) Energetics of quinone-dependent electron and proton transfers in Rhodobacter sphaeroides photosynthetic reaction centers. *Biochemistry* 44(1):82–96.

48. Diner BA, Schenck CC, De Vitry C (1984) Effect of inhibitors, redox state and isoprenoid chain length on the affinity of ubiquinone for the secondary acceptor binding site in the reaction centers of photosynthetic bacteria. *Biochim Biophys Acta* 766(1)9-20.

49. Lavergne J (1982) Mode of action of 3-(3,4-dichlorophenyl)-1,1-dimethylurea. Evidence that the inhibitor competes with plastoquinone for binding to a common site on the acceptor side of Photosystem II. *BBA - Bioenerg* 682(3):345–353.

50. Van Best JA, Duysens LNM (1975) Reactions between primary and secondary acceptors of Photosystem II in Chlorella Pyrenoidosa under anaerobic conditions as studied by chlorophyll a fluorescence. *Biochim Biophys Acta* 408(2):154–163.

51. Gunner MR, Tiede DM, Prince RC, Dutton PL (1982) Quinones as Prosthetic Groups in Membrane Electron-Transfer Proteins I: Systematic Replacement of the Primary Ubiquinone of Photochemical Reaction Centers wit Other Quinones. *Function of Quinones in Energy Conserving Systems*, ed Trumpower BL (Academic Press), pp 265–269.

52. Gopher A, et al. (1985) The effect of an applied electric field on the charge recombination kinetics in reaction centers reconstituted in planar lipid bilayers. *Biophys J*. 48(2):311–320.

53. Kleinfeld D, Okamura MY, Feher G (1984) Electron-transfer kinetics in photosynthetic reaction centers cooled to cryogenic temperatures in the charge-separated state: evidence for light-induced structural changes. *Biochemistry* 23(24):5780–5786.

54. Garbers A, Reifarth F, Kurreck J, Renger G, Parak F (1998) Correlation between protein flexibility and electron transfer from Q(A)/(-·) to Q(B) in PSII membrane fragments from spinach. *Biochemistry* 37(33):11399–11404.

55. Reifarth F, Renger G (1998) Indirect evidence for structural changes coupled with Q(B/-.) formation in photosystem II. *FEBS Lett* 428(3):123–126.

56. Krieger-Liszkay A, Rutherford AW (1998) Influence of herbicide binding on the redox potential of the quinone acceptor in photosystem II: relevance to photodamage and phytotoxicity. *Biochemistry* 37(50):17339–44.

57. Kern J, et al. (2005) Purification, characterisation and crystallisation of photosystem II from *Thermosynechococcus elongatus* cultivated in a new type of photobioreactor. *Biochim Biophys Acta* 1706(1–2):147–157.

58. Kato Y, Sugiura M, Oda A, Watanabe T (2009) Spectroelectrochemical determination of the redox potential of pheophytin a, the primary electron acceptor in photosystem II. *Proc Natl Acad Sci USA*. 106:17365–17370.

59. Sugiura M, et al. (2004) Site-directed mutagenesis of Thermosynechococcus elongatus photosystem II: the O2-evolving enzyme lacking the redox-active tyrosine D. *Biochemistry* 43(42):13549–63.

60. Sugiura M, Inoue Y (1999) Highly purified thermo-stable oxygen-evolving photosystem II core complex from the thermophilic cyanobacterium *Synechococcus elongatus* having His-tagged CP43. *Plant Cell Physiol* 40(12):1219–31.

61. Dutton PL (1971) Oxidation-reduction potential dependence of the interaction of cytochromes, bacteriochlorophyll and carotenoids at 77° K in chromatophores of *Chromatium D* and *Rhodopseudomonas gelatinosa*. *Biochim Biophys Acta* 226(1):63–80.

62. De Causmaecker S (2018) Bioenergetic Studies on the Quinone Electron Acceptors of Photosystem II. Dissertation (Imperial College London).

63. Mühlenhoff U, Chauvat F (1996) Gene transfer and manipulation in the thermophilic cyanobacterium *Synechococcus elongatus*. *Mol Gen Genet MGG* 252(1–2):93–100.

64. Porra RJ, Thompson WA, Kriedemann PE (1989) Determination of accurate extinction coefficients and simultaneous equations for assaying chlorophylls a and b extracted with four different solvents: verification of the concentration of chlorophyll standards by atomic absorption spectroscopy. *Biochim Biophys Acta* 975(3):384–394.

65. Nitschke W (2016) 2-electron redox chemistry. Available at: http://bip.cnrs-mrs.fr/bip09/2electron.html.

# Supplemental Information

PSII purification:

*T. elongatus* cells were grown in DTN medium (63) in 5 l Erlenmeyer flasks (2 l culture) in a rotary shaker (120 rpm) at 45 °C under continuous illumination from fluorescent white lamps (≈80 µmol of photons $m^{-2}$ $s^{-1}$). Typically, 18 l of cell culture were grown until $OD_{750}$=0.6. After harvesting by filtration with a Sartocon Hydrosart Microfiltration Cassette (0.2 µm; Sartorius Stedim UK Limited, Epsom, UK), the cells were centrifuged (11,280 g, 10 min) and washed once with buffer 1 (40 mM MES, 2.5 mM $MgCl_2$, 2.5 mM $CaCl_2$, 10% glycerol, 1 M betaine, 10 mM $NaHCO_3$, pH 6.5) and re-suspended in the same buffer, containing 0.2% ($^w/_v$) bovine serum albumin, 1 mM benzamidine, 50 µg $ml^{-1}$ DNase I and protease inhibitor cocktail (05 056 489 001; Roche, Basel, Switzerland) added, to a chlorophyll (Chl) concentration of ≈1.5 mg(Chl) $ml^{-1}$. The cells were ruptured by being passed twice through a high pressure (20 kpsi) cell disruption system (Constant Systems Ltd., Northants, UK). All subsequent steps were carried out in dim green light at 4 °C. Unbroken cells were removed by centrifugation (1500 g, 5 min, 4 °C). Thylakoids (1 mg(Chl) $ml^{-1}$, final concentration in buffer 1) were treated with 0.8% ($^w/_v$) *n*-dodecyl-β-maltoside (β-DM, Biomol, Germany). After brief (<10 min) and gentle mixing the suspension was centrifuged (60 min, 185000 g) to remove the non-solubilized material. Then, the supernatant was mixed with an equal volume of Probond Ni-resin (Invitrogen, Netherlands) that had been pre-equilibrated with buffer 2 (buffer 1 + 15 mM imidazole, 0.03% ($^w/_v$) β-DM) and applied to a column. The resin was washed with buffer 2 until the OD value of the eluate at ≈670 nm decreased below 0.05. Then, PSII core complexes were eluted with buffer 3 (buffer1 + 300 mM imidazole, 0.06% ($^w/_v$) β-DM, pH adjusted to 6.5 by adding concentrated HCl). The eluate was concentrated and washed using centrifugal filters (100 kDa Amicon Ultra-15, Millipore-Merck, Germany). PSII core complexes were re-suspended either in buffer 1 or in titration buffer (40 mM MOPS, 2.5 mM $MgCl_2$, 2.5 mM $CaCl_2$, 10% glycerol, 1 M betaine, 10 mM $NaHCO_3$, pH 7) at a Chl concentration of 1–1.5 mg(Chl) $ml^{-1}$ and stored in liquid $N_2$ until use. The estimate of Chl concentration was done by extracting the chlorophyll with methanol and by using an extinction coefficient of 79.95 $mg^{-1}$ ml $cm^{-1}$ at 665 nm (64).

Oxygen evolution activity of PSII samples was measured in buffer 1 supplemented with 0.5 mM 2,6-dichloro-*p*-benzoquinone (DCBQ) and 1 mM potassium ferricyanide (FeCN) at 2.5–10 µg(Chl) $ml^{-1}$ of PSII using a Clark-type electrode (Oxygraph, Hansatech Instruments Limited, UK) at 25 °C under saturating red light (>10,000 µmol $m^{-2}$ $s^{-1}$). The oxygen evolution activity was typically 2500–3500 µmol($O_2$) $mg(Chl)^{-1}$.

## Presence of Mn Cluster check by generation of $S_2$ state

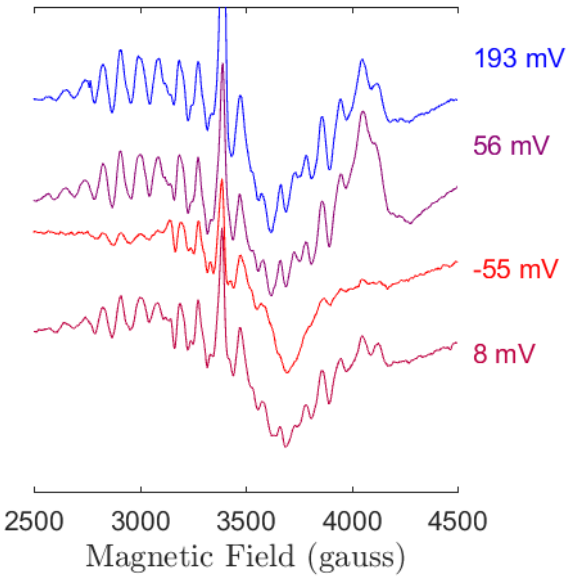


Figure S1: Generation of the $S_2$ multiline signal by illumination at 200 K. The multiline diminishes in the lowest potential sample but is reformed at higher potentials again.

All samples were exposed to light at 77 K to generate the g=1.66 signal. Thawing in darkness is done so that the electron from $Q_A$ can be transferred to $Q_B$. In the low-potential samples, however, this does not occur because $Q_B$ is reduced. When the samples were re-frozen and illuminated at 200 K, the samples containing PSII in which $Q_A^-$ remain reduced cannot do charge separation and therefore do not show EPR signal from the $S_2$ state.

## Fitting of experimental data.

To obtain the redox potentials of the two couples $Q_B/Q_B^{\bullet-}$ and $Q_B^{\bullet-}/Q_BH_2$ the experimental data was fit with the following expression.

$$[I] = \frac{[S]}{1+10^{(E-E_m-\frac{\Delta E}{2})\frac{F}{RT}}+10^{(E_m-E-\frac{\Delta E}{2})\frac{F}{RT}}} \quad \text{Eq. S1}$$

Here [I] is defined as the observed concentration of the intermediate semiquinone. [S] is the total quinone concentration,

$$E_m = (E_1+E_2)/2 \quad \text{Eq. S2}$$

and

$$\Delta E=E_1-E_2 \quad \text{Eq. S3}$$

For more details on how this relationship is derived see either Michaelis (34) or Nitschke (65)

## Calculation of dissociation constant.

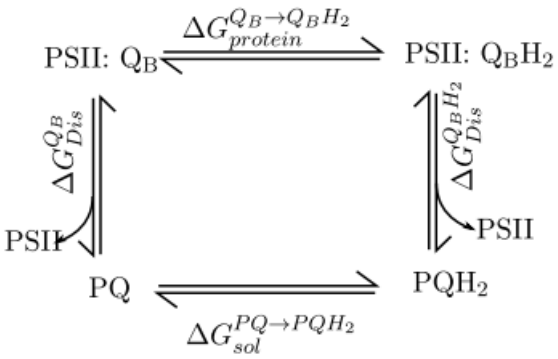


Figure S2: Relationship between the equilibrium dissociation energy ($\Delta G_{Dis}$) and redox energies of the reaction in solution and in the protein.

From Figure S2 it is apparent that

$$\Delta\Delta G_{protein} = \Delta G^{Q_B \rightarrow Q_B H_2}_{protein} - \Delta G^{PQ \rightarrow PQH_2}_{sol} = \Delta G^{Q_B}_{dis} - \Delta G^{Q_B H_2}_{dis} \quad \text{Eq. S5}$$

Because of the following relationship,

$$\Delta G_{dis} = RT \ln (K_{Dis}) \quad \text{Eq. S6}$$

Eq. S5 can be rearranged as follows

$$\Delta G^{Q_B \rightarrow Q_B H_2}_{protein} - \Delta G^{PQ \rightarrow PQH_2}_{sol} = RT \ln \left( \frac{K^{Q_B}_{Dis}}{K^{Q_B H_2}_{Dis}} \right) \quad \text{Eq. S7}$$

and the ratio of binding constants calculated:

$$\frac{K^{Q_B}_{Dis}}{K^{Q_B H_2}_{Dis}} = e^{\frac{\Delta G^{Q_B \rightarrow Q_B H_2}_{protein} - \Delta G^{PQ \rightarrow PQH_2}_{sol}}{RT}} \quad \text{Eq. S8}$$

## Re-evaluation of literature EPR titrations

EPR-redox titrations present in the literature were re-evaluated using the correct formula for the concentration of the intermediate semiquinone.

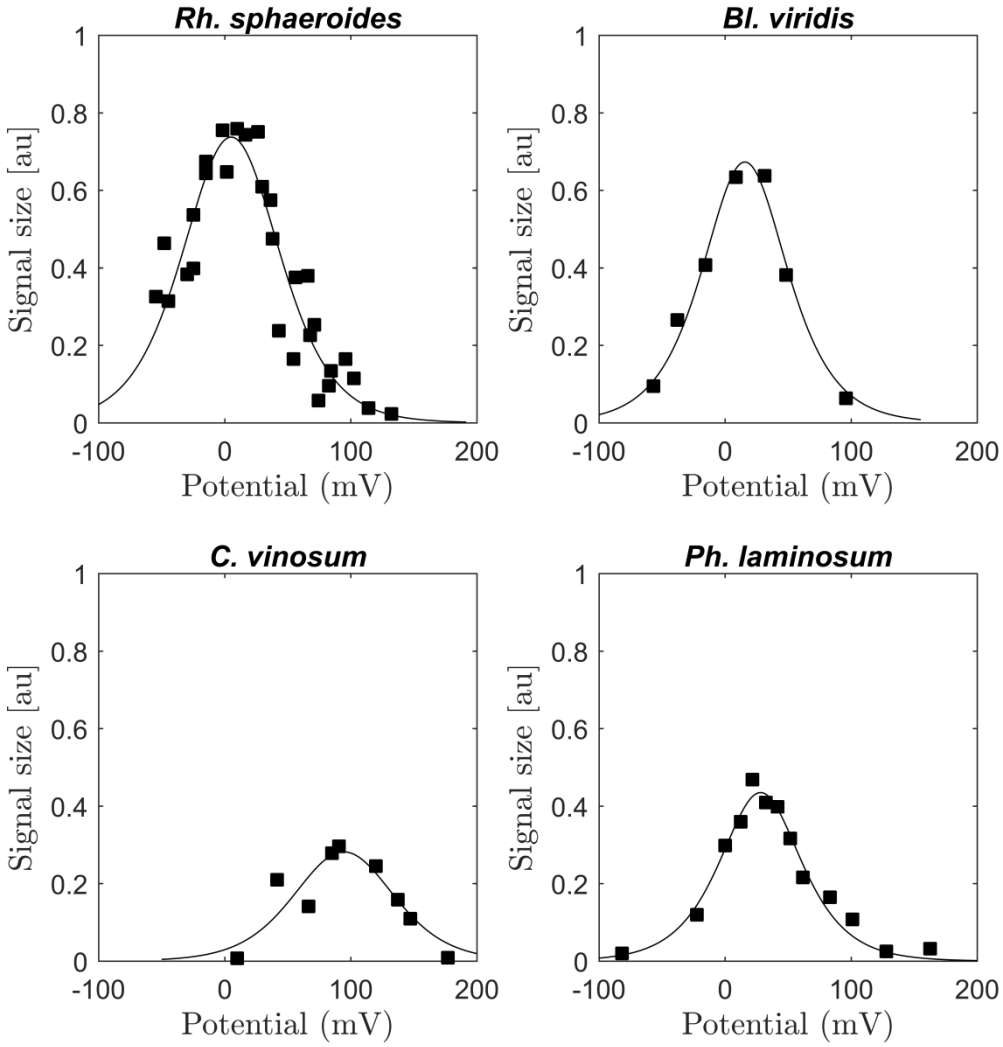


Fig S3: Literature titrations that were reanalysed. Data digitized from (26–28, 30).

Table S1. Values derived from fitting literature titrations.

| Organism | $E_m$ (peak pos.) [mV] | ΔE [mV] | % of total $Q_B$ [%] | $E_m$ @ pH 7 [mV] |
|---|---|---|---|---|
| *Rh. sphaeroides* pH 8 | 5±9 | 36±41 | 76 | 64 |
| *Bl. viridis* pH 8 | 16±11 | -5±89 | 29 | 75 |
| *Ch. vinosum* pH 7 | 94±31 | 45±115 | 58 | 94 |
| *Ph. laminosum* pH 8 | 28±8 | -21±82 | 27 | 86 |